Available online at www.sciencedirect.com
ScienceDirect
Ceramics International 38 (2012) 889–894
CERAMICS INTERNATIONAL
www.elsevier.com/locate/ceramint

Review paper

Synthesis of $SrAl_2O_4$ and $Sr_3Al_2O_6$ at high temperature, starting from mechanically activated $SrCO_3$ and Al_2O_3 in blends of 3:1 molar ratio

R. Saldaña Garcés *, J. Torres Torres, A. Flores Valdés

CINVESTAV-Unidad Saltillo, Carretera Saltillo-Monterrey Km. 13.5., PO Box 663, 25900 Ramos Arizpe, Coahuila, Mexico

Received 27 June 2011; received in revised form 8 August 2011; accepted 9 August 2011
Available online 17 August 2011

Abstract

The synthesis of strontium aluminates of the $SrAl_2O_4$ and $Sr_3Al_2O_6$ type using $SrCO_3$–Al_2O_3 blends was investigated. Blends 3:1 molar ratio of Al_2O_3 and mechanically activated $SrCO_3$ were prepared and conformed into pellets by uniaxial compression at 100 MPa. In an experimental stage, thermogravimetric analysis was used to investigate the isothermal decomposition of mechanically activated $SrCO_3$ powders in the blend, in the range of temperatures from 900 to 1100 °C. Then, samples were sintered at 1450 °C for several periods of time (4–36 h), and the products obtained were analyzed by X-ray diffraction and scanning electron microscopy. The results obtained showed that the formation of $Sr_3Al_2O_6$ starts after 4 h of heat treatment, and it is completed at 36 h. Moreover, other phase such as $SrAl_2O_4$ formed in small amounts in the samples sintered for 12 h. Kinetic measurements showed that the conversion of $SrCO_3$ into $Sr_3Al_2O_6$ follow two different reaction mechanisms, with different controlling steps. The first mechanism relates to the order of reaction model for the $Sr_3Al_2O_6$ phase formation, whereas the second mechanism relates to the nucleation and growth of these phase particles. The activation energy measured for both processes was 88.59 kJ and 54.06 kJ, respectively.

Keywords: Mechanical activation; Strontium aluminates; Thermally activated decomposition

Contents

1. Introduction

Strontium is found mainly as $SrSO_4$. This material is processed to obtain strontium carbonate, strontium nitrate [1,2], strontium oxide [3], or strontium chloride [4]. The strontium carbonate is widely used in several applications such as the fabrication of TV screens and in the manufacture of permanent magnets [5,6]. Recently, strontium aluminates have been extensively studied due to their wide range of applications.

When strontium aluminates are doped with Eu and Dy ions, phosphorescence properties are obtained [7–9]. Depending on the doped crystal structure of the strontium aluminate matrix, different colors could be reflected [10,11]. The phosphorescence properties attained in this way are useful for applications

* Corresponding author. Tel.: +52 844 4389600; fax: +52 844 4389600.
E-mail address: rocio.saldana@cinvestav.edu.mx (R.S. Garcés).

0272-8842/$36.00
doi:10.1016/j.ceramint.2011.08.021

such as watches fabrication, luminescent instruments, tools used in the dark, etc., where luminescent coatings produce required light for better vision [12,13].

Strontium aluminates can be also used in the fabrication of CO_2 sensors for the chemical or metallurgical industries, instead of sensors based on alkaline metals, as they can respond to temperatures of up to 1100 °C, for any change in the partial pressure of CO_2. This is due to their high properties such as chemical stability, mechanical resistance, corrosion resistance, and thermal and conductivity values [14,15]. For these reasons, they are highly employed also in the refractories industry.

The conventional process for obtaining strontium aluminates consists in mixing $SrCO_3$ and Al_2O_3 in stoichiometric amounts, then using temperatures greater than 1150 °C to attain $SrCO_3$ decomposition into SrO, forming in this way aluminates type compounds [1,3]. Temperatures can vary between 1200 and 1600 °C, with holding times of up to 144 h for solid state reactions.

A method of preparation of the starting materials by mechanical activation has proven to be a powerful tool for enhancing reactive sintering process, as less processing time and lower temperatures are required. Heinicke [16,17] define mechanical activation as a branch of chemistry, related to the physical and chemical transformations of the solids through the use of mechanical energy. One of the main effects of mechanical activation is the reduction in particles size, which has an important impact on the reaction rate [18]. As of the heat generated during milling, this treatment increase chemical reactivity of the solid not only by reducing particles size but also by promoted structural changes (lattice disorder, atomic mobility, point defects increase, etc.), generating high energy reaction zones, fractures and new surfaces [16,19–21].

Mechanochemical processing, which was initially intended to enhance ceramic strengthened alloys [4], has been successfully used to synthesize a wide range of nanosized ceramic powders, not only using high purity materials, but also starting from low grade materials. Chen et al. [22] used the high-energy ball milling treatment to prepare $SrAl_2O_4$. The milling was performed between 5 and 30 h. Other researchers observed that $SrAl_2O_4$ is the stable phase between 1000 and 1100 °C, so the transformation of this phase into pure compounds requires calcinations temperatures higher than 1250 °C, for completion [23].

In this study, $SrCO_3$ was ball milled between 30 and 180 min before mixing with Al_2O_3, in order to obtain pure $Sr_3Al_2O_6$ by solid-state reaction. The effects of the ball milling treatment on the microstructure of $SrCO_3$ and the formation of $Sr_3Al_2O_6$ were investigated using XRD and SEM techniques. The kinetics of the reactions was studied using thermogravimetric analysis at constant temperature, so it was possible to measure activation energy of different processes that occurred, as it will be discussed later.

2. Experimental

Powders of commercial Al_2O_3 (>99.9 purity) and $SrCO_3$ (>99.9 purity) with an average particle size of 50 μm, were used as starting materials. $SrCO_3$ was mechanically activated in a planetary mill (Analizette, Fritsch) for 30, 60, 90, 120, 150 and 180 min. The particle size distribution was measured using a Coulter LS100Q particle size analyzer.

For the analysis of the effect of mechanical activation on crystallite size, the most common technique employees the Scherrer equation. For determining crystallites size, first the X-ray diffraction pattern is obtained, where the peak broadening is used for determining such a value. This method is applied for crystallites size in the range from 3 to 100 μm [24]. The samples obtained were then analyzed by XRD to analyze the crystallite size in a Phillips diffractometer TW-3040 with Cu-K_α radiation ($\lambda = 0.15418$ nm). The crystallite sizes were calculated using Scherrer's equation:

$$D_{hkl} = \frac{0.9\,\lambda}{B\cos\theta} \quad (1)$$

where $D_{h\,k\,l}$ is the crystallites size, λ is the X-ray wavelength (0.15418 nm), θ is the Bragg's angle at which the peak is observed, measured in radians, and B is the full width of the diffraction line at half of the maximum intensity (FWHM).

Afterwards, a blend with a molar composition of 3:1 of $SrCO_3$ (mechanically activated) and Al_2O_3 was prepared. This blend was homogenized in a cylinder-shaped container using spinning rods and alumina balls for 4 h. Disc pellets, which were 2.5 cm in diameter, were formed by uniaxial pressing at 100 MPa.

In the first experimental stage, the samples were sintered in a tubular furnace Thermolyne 54500 at 1450 °C for several periods of time (4–36 h), and the heating rate used during sintering was also 10 °C/min. The products obtained were analyzed by X-ray diffraction and scanning electron microscopy (Phillips XL-30 ESEM). Scanning electron microscopy (SEM) was used to analyze microstructure formation via grain growth evolution and their semi-quantitative chemical composition.

Finally, thermogravimetric analysis was used for studying the decomposition kinetics of mechanically activated $SrCO_3$ in the blends with Al_2O_3. This was carried out in the range of temperatures from 900 to 1100 °C, during 4 h. Heating rate was fixed at 10 °C/min. The apparatus employed was a high temperature thermogravimetric analyzer Perkin Elmer, model TGA-7, using platinum crucibles.

3. Results and discussion

3.1. Mechanical activation of $SrCO_3$

In a previous work [26], samples of $SrCO_3$ were mechanically activated and the particle size distribution for the samples was analyzed. It was determined that over 45 min of milling, the particles size distribution did not change. Therefore, it is assumed that mechanical activation is effective after this period of time, so 45 min could be taken as the period of time at which mechanical activation starts. This is called 0 min activation time. The average size distribution of the particles is shown in Fig. 1.

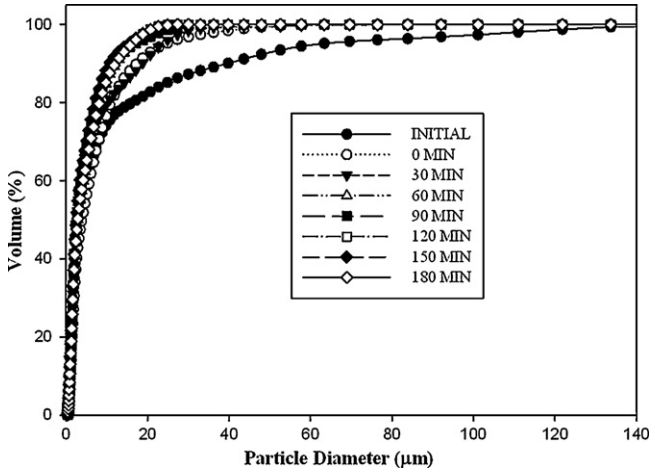

Fig. 1. Particle size distribution for mechanically activated $SrCO_3$ samples as a function of milling time.

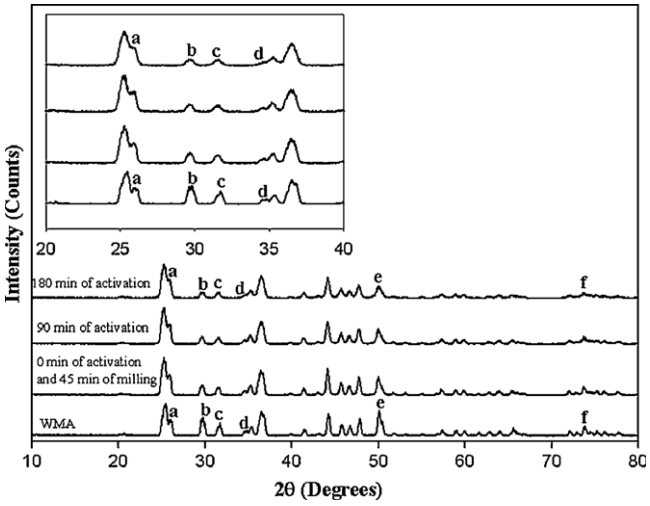

Fig. 2. XRD patterns of the $SrCO_3$ without mechanical activation and with mechanical activation for several times.

Fig. 2 shows a comparison between the XRD patterns of the $SrCO_3$ without mechanical activation (WMA) and those of the samples with mechanical activation. For the sake of comparison, the peaks corresponding only to the $SrCO_3$ are considered. As the mechanical activation time increases, the intensity of the peaks (a–f) decreased, whereas their width increased. The (f) peak during mechanical activation after 180 min tended to disappear. In conclusion, the distortion of the structure induced by mechanical activation is reflected in the line broadening and shift in reflections as well as the reduction of peak intensities (areas under the curves). To verify the effect of mechanical activation on crystallites size of $SrCO_3$ using the Scherrer's equation, the most intense peaks (1 1 1) in the X-ray diffraction pattern at the angle position (2θ) of 25.189° are selected. According to these results, the crystallite size decreased from 13.97 nm without mechanical activation to 10.39 nm with 180 min of mechanical activation.

3.2. Sintering of $3SrCO_3$–Al_2O_3 blend.

Fig. 3 shows the microstructure of the calcined powders at 1450 °C after 36 h with (c and d) and without mechanical activation (a and b). The samples without mechanical activation

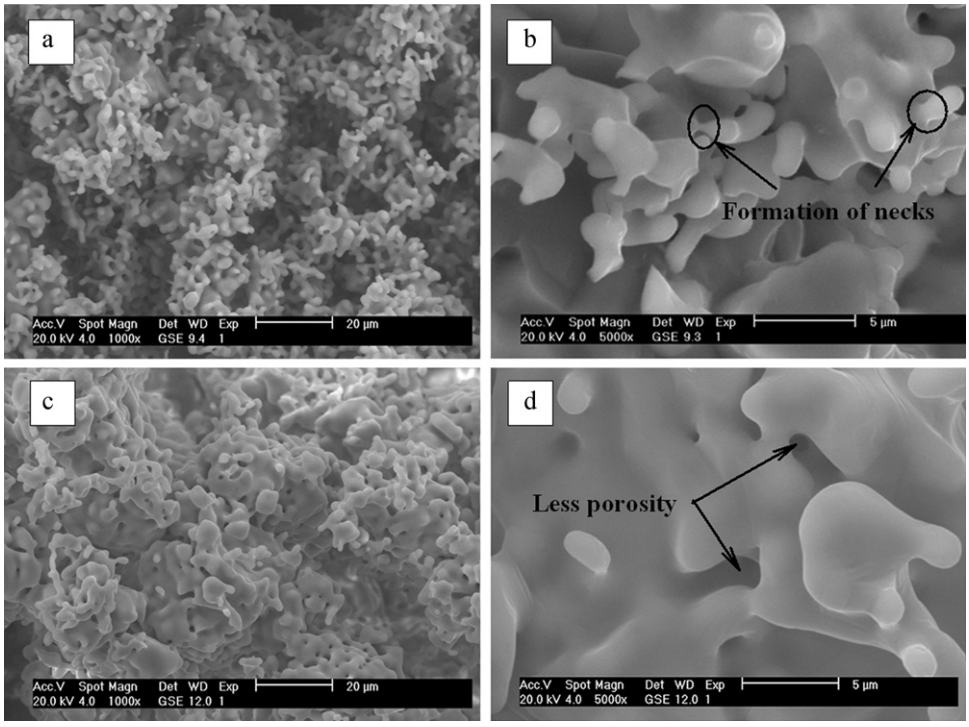

Fig. 3. Microstructure of the $3SrCO_3$–Al_2O_3 mixture calcined at 1450 °C for36 h: (a and b) without mechanical activation and (c and d) mechanically activated for 90 min.

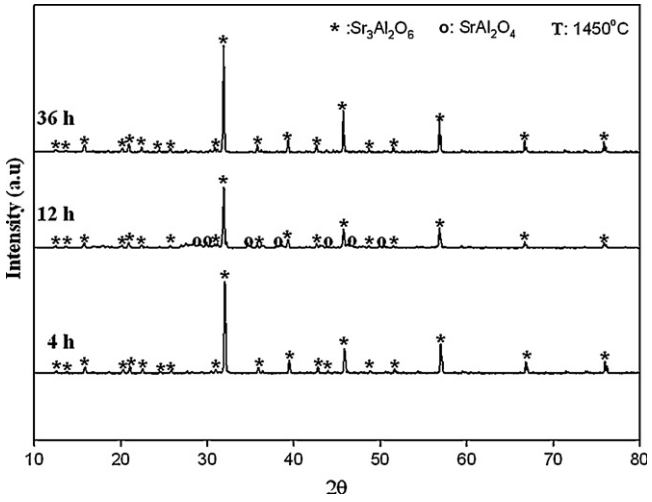

Fig. 4. XRD patterns corresponding to the sample of 3:1 $SrCO_3$:Al_2O_3 mechanically activated for 90 min and heat treated for 4, 12 and 36 h at 1450 °C.

presented the incipient formation of necks in the particles contact points where the mass transfer can occur and the surface energy is high. However, the material is highly porous, as shown in Fig. 3a. Sintering at 1450 °C for 36 h resulted in a porous microstructure with an average grain size of less than 1 μm (Fig. 3b).

The samples with mechanical activation presented a complete reaction in which the neck growth occurred completely and porosity decreased. Fig. 3c presents a microstructure with lower porosity and particles size are seen be larger by coalescence and was observed after 36 h of sintering (Fig. 3d).

3.3. Thermal behavior of a $3SrCO_3$–Al_2O_3 blend

Fig. 4 shows the XRD patterns corresponding to the sample, which contains $SrCO_3$ mechanically activated (for 90 min) after sintering at 1450 °C. $Sr_3Al_2O_6$ and $SrAl_2O_4$ were identified as the main phases. $Sr_3Al_2O_6$ was present after the 240 min sintering treatment. $SrAl_2O_4$ was present after 720 min sintering treatment. However, the intensity of the peaks corresponding to this phase decrease as the sintering time increased.

The microstructures of the calcined and sintered powders at 1450 °C are shown in Fig. 5. Fig. 5a shows an intermediate reaction stage, where a $SrAl_2O_4$ particle core is surrounded by the $Sr_3Al_2O_6$ phase. The reaction for this sample was incomplete, presenting a reaction layer of $Sr_3Al_2O_6$. This phase is considered as an intermediate aluminate formed during the synthesis of $Sr_3Al_2O_6$, as shown in the XRD pattern (Fig. 4). The reaction is completed at longer heat treatment times, as shown in Fig. 5b.

According to Chen et al. [22], $Sr_3Al_2O_6$ is obtained after 1800 min of mechanical activation and sintering at 1200 °C (they do not indicate holding time at this temperature). In this study, the time of mechanical activation was 3 h, and the sintering temperature was 1450 °C for 240–2160 min. Comparing the results of both investigations, it can be concluded that long mechanical activation times are not required to obtain this type of strontium aluminate. From the results of XRD analyses, a synthesis for the formation of the $Sr_3Al_2O_6$ can be proposed as follows.

The $SrAl_2O_4$ is formed after 4 h of sintering at 1450 °C. Then, at temperatures lower than 1100 °C, the SrO reacts with Al_2O_3 to give $SrAl_2O_4$ in a locally attained 1:1 M stoichiometric relationship, which can be attributed to the decomposition of strontium carbonate into SrO, which is represented as follows:

$$SrCO_3 = SrO + CO_2 \quad (2)$$

$$SrO + Al_2O_3 = SrAl_2O_4 \quad (3)$$

In contrast, at temperatures higher than 1100 °C, the $SrAl_4O_7$ was obtained, which is attributed to the chemical reaction between SrO and Al_2O_3 as a consequence of a 1:2 M stoichiometric relationship locally established, as shown by the next reaction:

$$SrO + 2Al_2O_3 = SrAl_4O_7 \quad (4)$$

However, this phase is not stable at this temperature, and it decomposes as follows:

$$SrAl_4O_7 = SrAl_2O_4 + Al_2O_3 \quad (5)$$

The residual SrO reacts with Al_2O_3 at higher temperatures (>1150 °C), forming the $Sr_3Al_2O_6$, as is presented by the next reaction:

$$3SrO + Al_2O_3 = Sr_3Al_2O_6 \quad (6)$$

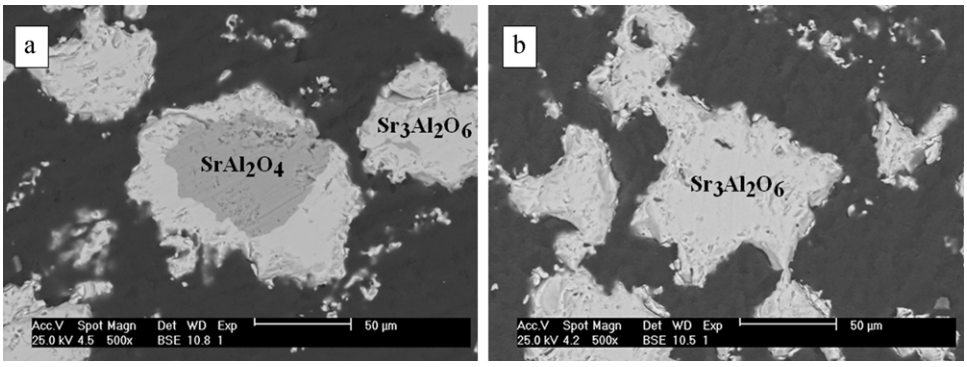

Fig. 5. Microstructure of the milled blend mechanically activated for 90 min and then calcined at 1450 °C for 12 h (a) and 36 h (b).

After 4 h of sintering at 1450 °C, the $Sr_3Al_2O_6$ and $SrAl_2O_4$ phases were observed. Thus, the entire reaction that represents the formation of aluminates is

$$5SrO + 3Al_2O_3 = 2SrAl_2O_4 + Sr_3Al_2O_6 \quad (7)$$

Therefore, under the treatment conditions described above, a mixture of phases of $Sr_3Al_2O_6$ and $SrAl_2O_4$ could be obtained.

3.4. Kinetics of $Sr_3Al_2O_6$ formation as $SrCO_3$ thermal decomposition in the presence of Al_2O_3

The initial objective of kinetic analysis is the identification of reaction rate equations which describe more appropriately the results of the reactions studied. For the selection of a kinetic model, different aspects must be taken into account, as follows: (1) fitting of the experimentally obtained values to the mathematically predicted values for the reacted fraction versus time, (2) the range of values over which the mathematically adjusted values fitting the experimentally obtained values is acceptable (it can be accepted that two different kinetic models could be applied in different ranges of reacted fraction to cover the entire range) and (3) validate the mathematically predicted values from a comparison with the values of a new set of experiments.

As is depicted in Table 1 [25], several kinetic models would exist to be employed on the study of solid state reactions.

According to the kinetic measurements performed in the system analyzed, the values of the reaction rate obtained were fitted to the models of Table 1. The best models fitting the kinetic values were; reaction order, first order (F_1) and nucleation and growth, energy law (P_n) of the $Sr_3Al_2O_6$ phase particles as a result of reaction (6).

The order of reaction model (F_1) describes the first part of the considered system, from 0 to 110 min, while the model of nucleation and growth (P_n) describes the second part, from 110 min or greater.

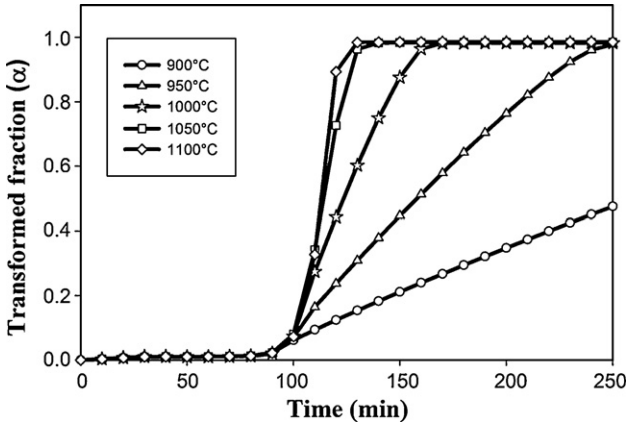

Fig. 6. Plots of transformed fraction (α) versus time for $SrCO_3$ and Al_2O_3 at various temperatures.

The transformed fraction α was calculated using the following equation:

$$\alpha = \frac{m_0 - m_t}{m_0 - m_f} \quad (8)$$

where m_0 is initial mass, m_t is the actual loss or gain of mass, and m_f is the total loss or gain of mass.

Fig. 6 shows the corresponding curves of transformed fraction of α as a function of temperature. The mass fraction of $Sr_3Al_2O_6$ increases as the temperature increases, and is very close to 1.

Fig. 7 is a comparison of the two models fitting the experimental results, where the overall behavior of the $Sr_3Al_2O_6$ formation can be distinguished.

During the first stage, the thermal decomposition of $SrCO_3$ occurs, as is shown in Eq. (2), which initiates chemical reaction between SrO and Al_2O_3. Immediately, the nucleation and growth of $Sr_3Al_2O_6$ particles occurs. From the curves of (α)

Table 1
Differential and integral functions of the several kinetic models employed for studying solid state reactions [25].

Kinetic model	Differential form $f(\alpha) = (1/k)\ (d\alpha/dt)$	Integral form $g(\alpha) = kt$
Nucleation and growth models		
Energy law (P_n) $1 \le n \le 3$	$n\alpha^{(n-1)/n}$	$\alpha^{(1/n)}$
Exponential law (E_1)	α	$\ln \alpha$
Avrami–Erofeev (A_2)	$2(1-\alpha)[-\ln(1-\alpha)]^{1/2}$	$[-\ln(1-\alpha)]^{1/2}$
Avrami–Erofeev (A_3)	$3(1-\alpha)[-\ln(1-\alpha)]^{1/3}$	$[-\ln(1-\alpha)]^{1/3}$
Avrami–Erofeev (A_4)	$4(1-\alpha)[-\ln(1-\alpha)]^{1/4}$	$[-\ln(1-\alpha)]^{1/4}$
Geometrical contraction models		
Phase boundary (R_n) $1 \le n \le 3$	$n(1-\alpha)^{1/n}$	$1-(1-\alpha)^{1/n}$
Contracting area (R_2)	$2(1-\alpha)^{1/2}$	$1-(1-\alpha)^{1/2}$
Contracting volume (R_3)	$3(1-\alpha)^{2/3}$	$1-(1-\alpha)^{1/3}$
Diffusion models		
Unidimensional diffusion (D_1)	$1/2\alpha$	α^2
Two-dimensional diffusion (D_2)	$[-\ln(1-\alpha)]^{-1}$	$[(1-\alpha)\ln(1-\alpha)] + \alpha$
Three-dimensional diffusion (D_3)	$3/2(1-\alpha)^{2/3}(1-(1-\alpha)^{1/3})$	$[1-(1-\alpha)^{1/3}]^2$
Ginstling–Brounshtein (D_4)	$3/2[(1-\alpha)^{-1/3}-1]^{-1}$	$1-(2\alpha/3)-(1-\alpha)^{2/3}$
Reaction-order models		
Zero-order (F_0)	1	α
First-order (F_1)	$(1-\alpha)$	$-\ln(1-\alpha)$
Second-order (F_2)	$(1-\alpha)^2$	$[1/(1-\alpha)]-1$
Third-order (F_3)	$(1-\alpha)^3$	$[1/(1-\alpha)^2]-1$

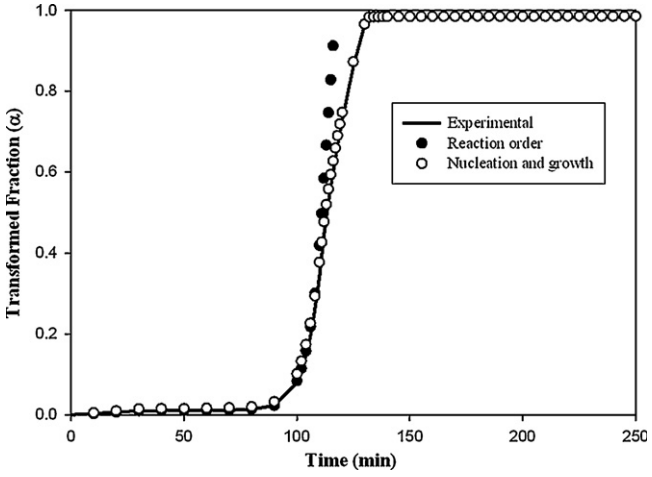

Fig. 7. Comparison of the two models fitting the experimental results.

versus time in Fig. 7, the values of the rate constants for each one of the temperatures were determined. From a plot of ln k versus 1/T, the activation energies of these processes were obtained, using the Arrhenius equation:

$$k = A \exp\left(\frac{-Ea}{RT}\right) \tag{9}$$

Two values of activation energy were calculated; the first one corresponds to the model of order of reaction (F_1), for the time interval from 0 to 110 min, while the second one corresponds for the nucleation and growth model (P_n) for the time interval of 110 min and greater. These values were the following:

Reaction order : 88.59 kJ (10)

Nucleation and growth : 54.06 kJ (11)

4. Conclusions

Strontium aluminates of the $SrAl_2O_4$ and $Sr_3Al_2O_6$ type were synthesized by solid-state reaction. Starting from mechanically activated $SrCO_3$ in blends 3:1 molar with Al_2O_3. X-ray diffraction and SEM analyses confirmed the presence of strontium aluminates phases, demonstrating that mechanical activation is a useful method to obtain $SrAl_2O_4$ and $Sr_3Al_2O_6$ by solid-state reaction, which can shorten processing times compared to conventional processes. Kinetics measurements allowed to determine the main governing mechanisms of reaction; chemical reaction (Ea = 88.59 kJ) for time interval from 0 to 110 min and nucleation and growth (Ea = 54.06 kJ) for time interval from 110 and greater minutes.

Acknowledgement

The financial support from the CONACyT is gratefully recognized (project ECO-2006-C01-52822).

References

[1] N. Ahmad, A. Chang, Thermodynamic Data on Metal Carbonate and Related Oxides, The Metallurgical Society of AIME, University of Wisconsin, Madison-Wisconsin, 1982, pp. 188–198.
[2] K. Fitzner, Z. Panek, Termochim. Acta 113 (1987) 359–368.
[3] D. Arvanttidis, S. Seerharaman, D. Sichen, Estudio de la descomposición termodinámica de $BaCO_3$ y $SrCO_3$, in: W. Hale (Ed.), Light Metals, The Minerals Metals and Materials Society, 1996, pp. 1191–1199.
[4] M. Iwai, M. Toguri, The leaching of celestite in sodium carbonate solution, Hydrometallurgy (1989) 87–100.
[5] R.E. Kirk, D.F. Othmer, Estroncio Compuestos. Enciclopedia de la tecnología química, tomo VII, in: UTHEA, 1962, pp. 472–476.
[6] J. Griffiht, Celestite: new production and processing developments, Ind. Miner. (November) (1985) 10–11.
[7] T. Katsumata, K. Sasajima, T. Nabae, S. Komuro, T. Morikawa, Characteristic of strontium aluminate crystal used for long duration phosphors, J. Am. Ceram. Soc. 81 (1998) 413–416.
[8] X. Luo, W. Cao, Z. Xiao, Investigation on the distribution of rare earth ions in strontium aluminate phosphors,, J. Alloys Compd. 416 (2006) 250–255.
[9] C. Chang, Z. Yuang, D. Mao, Eu2+ activated long persistent strontium aluminate nano scaled phosphor prepared by precipitation method, J. Alloys Compd. 415 (2006) 220–224.
[10] H. Takasaki, S. Tanabe, T. Hanada, Long-lasting afterglow characteristics of Eu, Dy co-doped $SrO–Al_2O_3$ phosphor, J. Ceram. Soc. Jpn. 104 (1995) 322–326.
[11] K. Fukuda, K. Fukushima, Crystal structure of hexagonal $SrAl_2O_4$ at 1073 K, J. Solid State Chem. 178 (2005) 2709–2714.
[12] T. Matsuzawa, Y. Aoki, N. Takeuchi, Y. Murayama, A new long phosphorescent phosphor with high brightness $SrAl_2O_4$:Eu and Dy, J. Electrochem. Soc. 143 (8) (1996) 2670–2673.
[13] Z.C. Wu, J.X. Shi, J. Wang, H. Wu, Q. Su, M.L. Gong, Synthesis and luminescence properties of $SrSl_2O_4$:Eu^{2+} green-emitting phosphor for white leds, Mater. Lett. 60 (2006) 3499–3501.
[14] Goto Takashi, Gange He, Takayuki Narushima, Yasutaka Iguchi, Application of Srβ-alumina solid electrolyte to a CO_2 gas sensor, Solid State Ionics 156 (2003) 329–336.
[15] Capron Mickael, Douy André, Strontium dialuminate $SrAl_4O_7$: synthesis and stability, J. Am. Ceram. Soc. 85 (12) (2002) 3036–3040.
[16] P. Baláz, Extractive Metallurgy of Activated Minerals, Elsevier Science BV, 2000.
[17] G. Heinicke, Tribochemistry, Akademie-Verlag, Berlin, 1984.
[18] Fernandez-Bertran, J. Mechanochemistry: an overview, Pure Appl. Chem. 4 (1999) 581–586.
[19] V.V. Boldyrev, S.V. Pavlov, E.L. Goldberg, Interrelation between fine grinding and mechanical activation, Int. J. Miner. Process. 44–45 (1990) 180–185.
[20] V.V. Boldyrev, Reactivity of solids, J. Therm. Anal. 40 (1993) 1041–1062.
[21] P.G. McCormick, F.H. Froes, The fundamentals of mechanochemical processing, JOM (November) (1998) 61–65.
[22] G. Chen, D. Niu, X. Liu, Preparation of $SrAl_2O_4$ from an oxide mixture via a high-energy ball milling, J. Alloys Compd. 399 (2005) 280–283.
[23] Y.K. Song, S.K. Choi, H.S. Moon, T.W. Kim, S.I. Mho, H.L. Peak, Phase studies of $SrO–Al_2O_3$ by emission signatures of Eu^{2+} and Eu^{3+}, Mater. Res. Bull. 32 (1997) 337–341.
[24] V. Uvarov, I. Popov, Materials Characterization, vol. 58, Elsevier, 2007, pp. 883–891.
[25] M.E. Brown, Handbook of Thermal Analysis and Calorimetry, 1st ed., Elsevier, 1998.
[26] Mendoza del Angel Humberto, Análisis del comportamiento a alta temperatura durante el proceso de sinterización reactiva del sistema $SrO–SrSO_4$ pre-tratado con activación mecánica, Tesis de Maestría CINVESTAV-IPN Unidad Saltillo, México, 2003, pp. 42–43.